



# Hydrophobic behaviour of reduced graphene oxide thin film fabricated via electrostatic spray deposition

RAMIZ ZULKHARNAY<sup>1,2,\*</sup>, ORAL UALIBEK<sup>2</sup>, OLZAT TOKTARBAIULY<sup>2</sup>  
and PAUL W MAY<sup>1</sup>

<sup>1</sup>School of Chemistry, University of Bristol, Cantock's Close, Bristol BS8 1TS, UK

<sup>2</sup>National Laboratory Astana, Nazarbayev University, Nur-Sultan 010000, Kazakhstan

\*Author for correspondence (ramiz.zulkharnay@bristol.ac.uk)

MS received 19 July 2020; accepted 20 November 2020

**Abstract.** Graphene-based materials such as graphene oxide (GO) and chemically reduced graphene oxide (rGO) thin films have been fabricated using electrostatic spray deposition (ESD), followed by thermal annealing under Ar/H<sub>2</sub> atmosphere. The thickness and surface morphology of thin films of GO and rGO on silicon substrates were controlled by varying deposition time and content of GO/rGO in tetrahydrofuran (THF) solution. Here, we present a comparative analysis between GO and rGO thin films. Water contact angle (WCA) measurements of these thin films were ~88° for the GO films and >127° for the rGO films. We discuss how their hydrophobic behaviour is influenced by removal of oxygen-containing functional groups during the reduction process.

**Keywords.** Carbon materials; electrostatic spray deposition; reduced graphene oxide; surfaces; thin films.

## 1. Introduction

Graphene is a smooth single layer of *sp*<sup>2</sup>-bonded carbon atoms closely assembled into a hexagonal arrangement on a two-dimensional (2D) network, creating the main building unit for carbon materials of any dimensionality [1–3]. Full oxidation of graphene produces graphene oxide (GO), which can then be chemically reduced to a partially oxidized material known as reduced graphene oxide (rGO) [4]. Graphene-, GO- and rGO-based hydrophobic layers have attracted considerable attention due to their possible applications in self-cleaning surfaces [5], reducing oxidation/corrosion [6], oil–water separation [7,8], non-wetting transparent flexible electrodes [9] and bacterial antifouling [10]. The development of such surfaces essentially requires the combination of low surface tension with surface roughness at the nano- and microscale [11,12].

To enhance the surface functionalization of graphene-based materials, scientists have used techniques such as chemical vapour deposition [13], plasma etching [14], chemical treatment [15], dip [16] and spin coating [17]. However, the challenging issue in this field remains with the control of the surface properties during the fabrication process. Most of those techniques are laborious, costly and inappropriate for large-scale manufacturing. In contrast, electrospray deposition (ESD) is a versatile method for

fabricating hydrophobic thin films, which is affordable, scalable and compatible with other coating approaches. Moreover, being relatively unstudied for the deposition of carbon materials, it is a promising technique to satisfy coating requirements. In ESD, the use of an electric field directly contributes to the precise control of the droplet movement towards the desired substrate; thus, forming uniform and mask-less thin films with high efficiency over 80% [18–20]. In comparison, when using uncharged conventional spray methods nearly half of the deposition material (40–50%) misses the substrate and is wasted [21].

A selection of (mainly polar) solvents plays a key role in the ESD technique. Due to the attachment of oxygen-containing functional groups (hydroxyl, carbonyl and carboxyl) to the carbon skeleton, chemically synthesized GO and rGO can be adapted to be readily soluble in typical polar solvents. The dispersion features of GO and rGO have been previously studied with an extensive variety of organic solvents [22]. Based on these findings, in this study, tetrahydrofuran (THF) was chosen as the solvent because of its beneficial physicochemical properties, such as surface tension, dipole moment and Hildebrand solubility parameters.

Here, we have investigated the single-step preparation of GO and rGO thin films by ESD. Both graphene-based

*Electronic supplementary material:* The online version of this article (<https://doi.org/10.1007/s12034-021-02381-x>) contains supplementary material, which is available to authorized users.

materials were deposited onto silicon substrates, and film characteristics, including hydrophobic and structural properties, surface morphology, thickness and thermal stability, were determined.

## 2. Experimental

### 2.1 Materials

Graphite powder (<20  $\mu\text{m}$ , 99.5%), sodium nitrate (99%), sulphuric acid (98%), potassium permanganate (99%), hydrogen peroxide (30%), monohydrate hydrazine (98%), THF (99%) and undoped silicon wafers (100) were procured from Sigma-Aldrich. Hydrochloric acid (10%) was supplied by Merck.

### 2.2 Synthesis of GO

GO was produced using a modified Hummers' method [23,24]. Graphite powder (1 g) was treated by vigorous stirring at 35°C in an anhydrous mixture of  $\text{NaNO}_3$  (0.5 g),  $\text{H}_2\text{SO}_4$  (23 ml), and  $\text{KMnO}_4$  (3 g) for 12 h, followed by addition of deionized water (46 ml) and oxidation by  $\text{H}_2\text{O}_2$  (2.5 ml). This produced a yellowish-brown graphite-oxide solution, which was then thoroughly washed with 10% HCl (aq.) and then with deionized water several times until the pH stabilized at  $\sim 7$ . This homogenous solution was ultrasonically treated for 30 min to exfoliate the graphite oxide into GO. To exclude precipitates of GO, the solution was centrifuged at 3500 rpm for 40 min. The resulting greyish-black product was filtered using glass funnel filters with sintered glass discs (10–40  $\mu\text{m}$  pore size) and dried in a vacuum oven at 80°C for 2 h.

### 2.3 Preparation of rGO

Preparation of rGO was achieved using a chemical reduction via monohydrate hydrazine ( $\text{N}_2\text{H}_4\cdot\text{H}_2\text{O}$ ) [24]. Initially, a colloidal suspension of GO in deionized water ( $5 \text{ mg ml}^{-1}$ ) was obtained by placing the homogenous GO solution into an ultrasonic bath for 3 h, followed by adding  $\text{N}_2\text{H}_4\cdot\text{H}_2\text{O}$  (2  $\mu\text{l}$  for 5 mg of GO) and then stirring with a teflon-coated magnetic rod, while heating in an oil bath at 70°C for 14 h. This led to a black precipitation of rGO. Filtration and drying procedures were performed as for GO.

### 2.4 Fabrication of GO and rGO thin films

GO and rGO thin films were deposited onto silicon substrates by ESD. The Si substrates were first cleaned using acetone and isopropanol, and then placed in the ESD chamber on an electrically grounded platen and heated to 250°C. Colloidal suspensions of GO and rGO were then prepared separately by dispersing 0.2 mg in 100 ml THF using an ultrasonic bath. The chosen colloidal suspension was placed into a container, which allowed the liquid to spray through a metal nozzle at a flow rate of  $\sim 5 \text{ ml h}^{-1}$ . The opening of the nozzle was located at fixed 5 cm distance from the substrate platen. When a direct current bias of 7.5 kV was applied between the nozzle and the grounded platen, the liquid suspension sprayed towards the hot substrate coating it in a thin film, which dried rapidly as the volatile liquid evaporated. This spraying procedure was carried out for 20 min. The coated substrates were then annealed in a tube oven at 500°C under  $\text{Ar}/\text{H}_2$  (5:1) atmosphere for 2 h followed by cooling to room temperature. A fabrication route for graphene-based materials using the ESD technique followed by thermal annealing is depicted in figure 1.

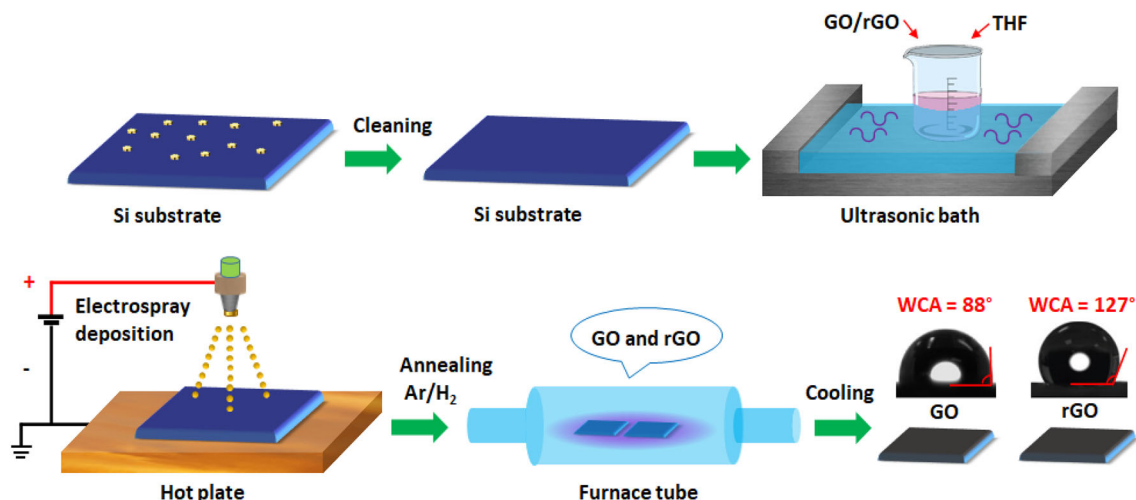


**Figure 1.** A schematic illustration of the experimental design for the preparation of hydrophobic graphene-based thin films.

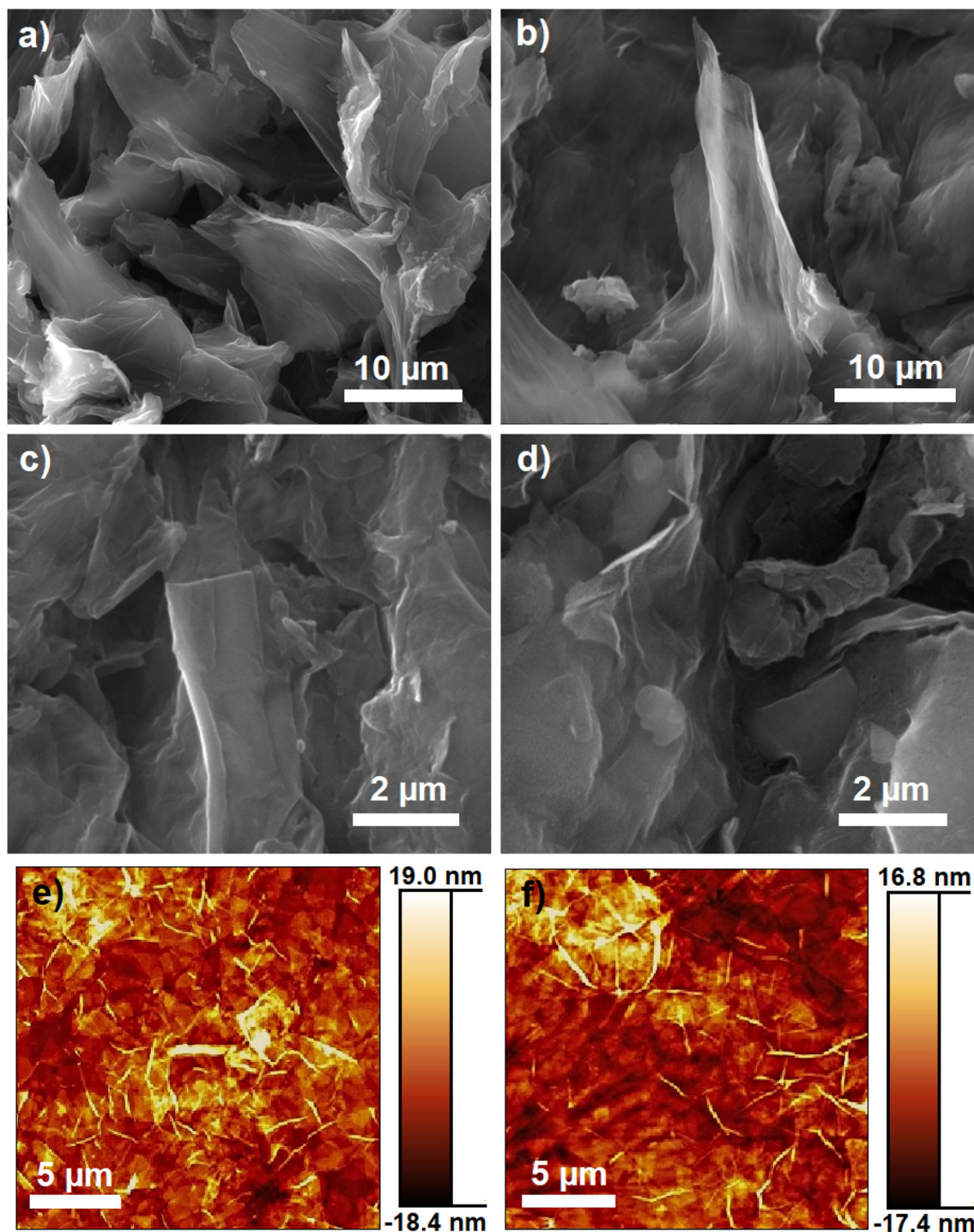


**Figure 2.** SEM and AFM images of as-deposited GO (a, c, e) and rGO (b, d, f) thin films at different magnifications.

### 2.5 Characterization

The surface morphology and elemental analysis of the GO and rGO thin films were determined via scanning electron microscopy (SEM) combined with energy-dispersive X-ray analysis (EDX) in a JEOL JSM-IT300 SEM system. Atomic force microscopy (AFM) imaging was performed

using a Bruker Multimode VIII microscope with Nanoscope V controller functioning under PeakForce Tapping mode over a scanning area of  $3 \times 3 \mu\text{m}^2$ . A Bruker Dektak XT Profilometer was employed to examine the thickness of the thin films using Vision 64 software for data collection. Fourier-transform infrared (FTIR) spectra ( $500\text{--}4000 \text{ cm}^{-1}$ ) were recorded using a Perkin-Elmer

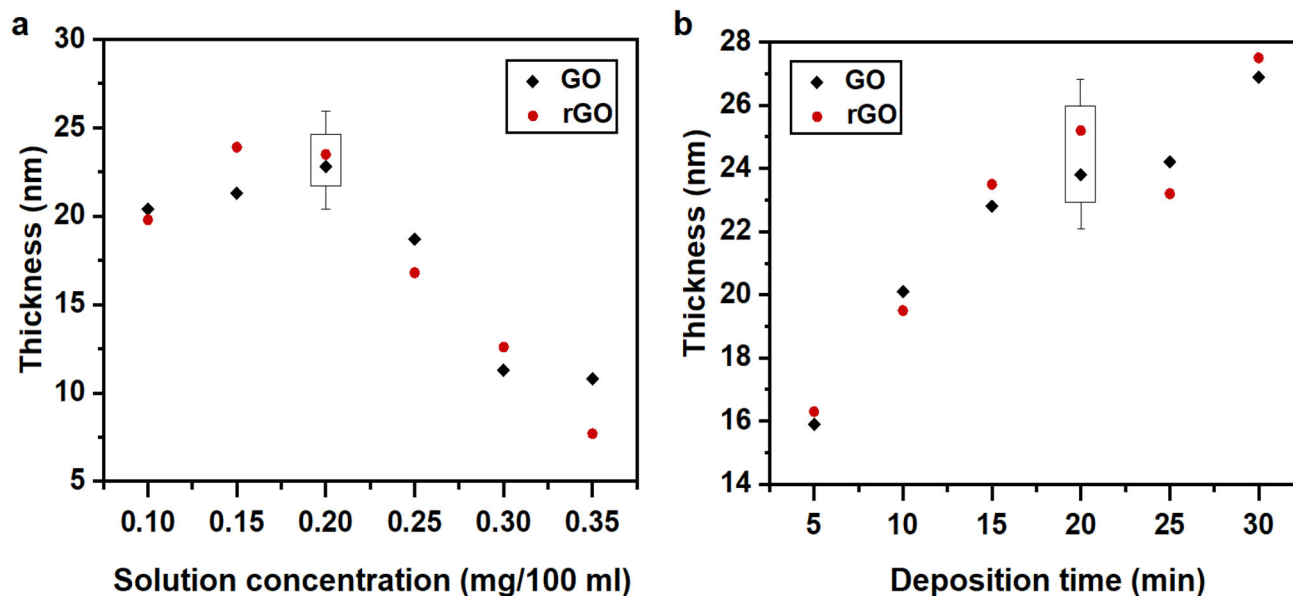


**Figure 3.** Optimization of ESD deposition for GO and rGO thin films on Si substrates  $1 \text{ cm}^2$  in area. (a) Thickness vs. solution concentration for the deposited films with coating time of 15 min. (b) Thickness measurements of both films at different deposition times with composition fixed at 0.2 mg per 100 ml.

**Table 1.** Thickness measurement summary of the deposited GO and rGO thin films via Dektak XT Profilometry and AFM.

Material	Thickness (nm)	
	Profilometer	AFM
GO	$23.8 \pm 3.5$	$24.1 \pm 2.9$
rGO	$25.2 \pm 4.1$	$25.9 \pm 3.7$

Spectrum One spectrometer. Raman spectra ( $500\text{--}3000 \text{ cm}^{-1}$ ) were taken using a Renishaw 2000 Laser Raman spectrometer ( $\text{Ar}^+$  laser,  $514 \text{ nm}$  excitation) at room temperature. X-ray diffraction (XRD) analysis was observed within the glancing-angle range  $5^\circ\text{--}50^\circ$  using a Siemens D500 X-ray diffractometer equipped with a  $\text{Cu K}\alpha$  radiation ( $0.154 \text{ nm}$ ). Thermogravimetric analysis (TGA) was performed by a Mettler Toledo Star System instrument in  $\text{N}_2$  atmosphere from room temperature to  $1000^\circ\text{C}$  with a heating rate of  $10^\circ\text{C min}^{-1}$ . Water contact angle (WCA) measurements were carried out by a Krüss DSA100 drop-shape analyser using a  $0.25 \mu\text{l}$  water droplet at room temperature.

### 3. Results and discussion

SEM and AFM images of the deposited GO and rGO thin films are shown in figure 2. These show that both film types are composed of randomly arranged few-layer graphene

sheets containing ripples and wrinkles. Noticeably, both film types form a continuous coating onto the Si substrates. Some of the rGO sheets (figure 2b and d) appear thinner and more transparent than those in the GO film (figure 2a and c), with average dimensions of  $8 \times 10 \mu\text{m}$ . Further, the as-deposited rGO film has a rougher pattern with numerous micron-sized holes (figure 2d). Both of these observations suggest significant etching of the rGO film. EDX spectra (see supplementary figure S1 and table S1) reveal that the C:O atomic ratio of rGO is significantly increased compared to that in GO, providing evidence that the reduction with hydrazine monohydrate has been, at least partially, successful.

The thickness of the thin films was adjusted by varying the concentration of GO/rGO in THF and the deposition time (figure 3). The outlined solution concentration and deposition time were chosen as optimal conditions for the deposition. Due to the dispersibility features of both graphene-based materials in THF, there is a gradually declining trend in the thickness for concentrations  $>0.2 \text{ mg per } 100 \text{ ml}$  (figure 3a). By contrast, the thickness dependence of the deposition time (figure 3b) shows moderate increase in the film thickness with time. The data points for both samples after 25 min deposition seem anomalously small and should probably be treated with caution or discounted as outliers. All related measurements were performed using a Dektak XT Profilometer. These measurements of the thickness are consistent with those from AFM studies, as summarized in table 1.

Confirmation of the appreciable structural alterations arising from the chemical reduction of GO can be seen in figure 4. There are two prominent Raman bands (D and G)

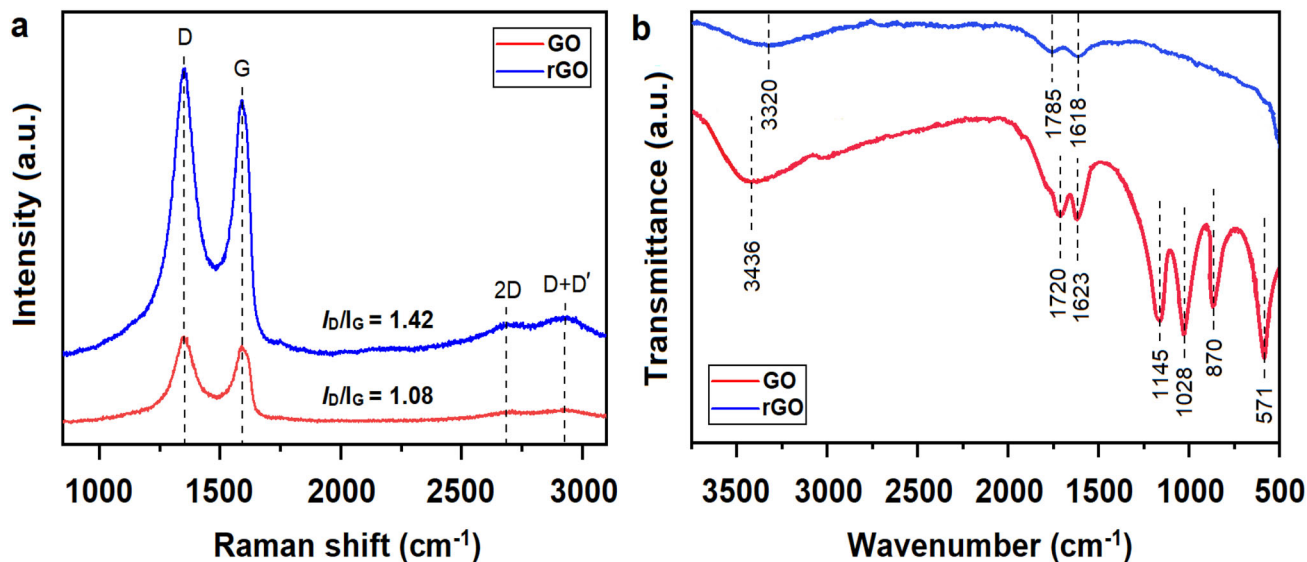


**Figure 4.** Structural studies of the GO and rGO films. (a) Raman spectra with the D and G peaks labelled along with their intensity ratios  $I_D/I_G$ . (b) FTIR spectra exhibiting the bands from oxygen-containing functional groups. GO (red, lower) and rGO (blue, upper) films.

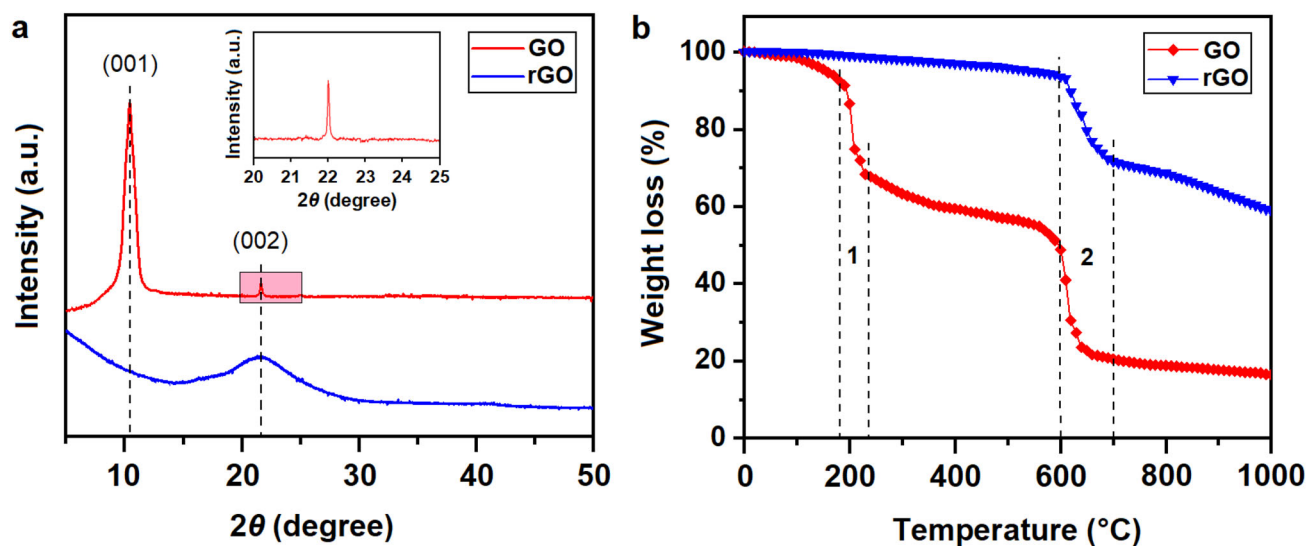


**Figure 5.** Structural and thermal analysis of the GO and rGO films. (a) XRD patterns showing the peaks from the (001) and (002) planes. The inset is a magnified view of the region around the (002) facet for GO. (b) TGA curves depicting weight-loss events at  $\sim 180$ – $230^\circ\text{C}$  and  $\sim 600$ – $700^\circ\text{C}$ .

in both graphene-based materials shown in figure 4a. The D band  $\sim 1345\text{ cm}^{-1}$  corresponds to structural defects in the graphene network, while the G band at  $\sim 1590\text{ cm}^{-1}$  is related to vibrations of  $sp^2$ -hybridized carbon atoms and the  $E_{2g}$ -symmetry phonon mode at the Brillouin zone centre. The intensity ratio of the D and G bands ( $I_D/I_G$ ) is a useful measure of structural disorder and correlates to the average size of graphene clusters. Successful reduction of GO to rGO is shown by the increase of  $I_D/I_G$  ratio from 1.08 to 1.42, suggesting that the reduction process has significantly

enhanced the  $sp^2$  cluster size in rGO [25]. For rGO, two additional bands appear in the range from 2600 to  $3000\text{ cm}^{-1}$ , which attributed to 2D and D + D'. However, due to their low intensity, both peaks are usually disregarded in the context of such studies. The 2D peak is generally related to the thickness of separate graphene layers, and is assigned to the second order of the D band arising from lattice vibrations of the two-phonon mode. By contrast, the D + D' peak (frequently labelled as the D + G in the literature) is related to the appearance of defects in

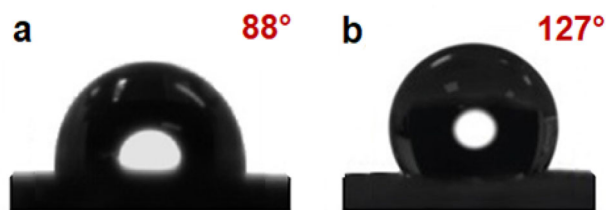


**Figure 6.** Images of the water droplet shapes for (a) GO and (b) rGO films, with their respective contact angles.

the sample. The observation of this  $D + D'$  peak provides additional evidence that some surface modification has occurred in our rGO films [26].

The FTIR spectrum of the GO film (figure 4b) shows that there are various bands from different oxygen-containing functional groups. The broad absorption peak at  $3436\text{ cm}^{-1}$  corresponds to the O–H stretching vibration. The twin bands at  $1720$  and  $1623\text{ cm}^{-1}$  are assigned, respectively, to the carbonyl C=O stretching vibration, and to the combination of the C=C aromatic stretching vibration of  $sp^2$ -hybridized atomic domains and the O–H bending vibration of absorbed water. Peaks at  $1145$ ,  $1028$  and  $870\text{ cm}^{-1}$  are due to C–C, C–O and C–O vibrations in the antisymmetric coupled stretching modes of aromatic groups, respectively. The strong band at  $571\text{ cm}^{-1}$  relates to C–O–C stretching, which is in good agreement with a previous study [27]. For rGO, the intensities of the peaks from all the above-mentioned oxygen functional groups are considerably reduced and slightly shifted, while the strong peaks around  $571$ ,  $870$ ,  $1028$  and  $1145\text{ cm}^{-1}$  have disappeared. A brief summary of the adsorption bands with their relative positions in the FTIR spectra is given in supplementary table S2.

Figure 5a shows XRD patterns from both films. For the GO film, a sharp diffraction peak at  $2\theta = 10.52^\circ$  ( $d = 0.84\text{ nm}$ ) relating to the (001) plane indicates an increase in the interlayer separation compared to that from pure graphene due to the presence of oxygen functional groups. There is a tiny peak at  $2\theta = 22.08^\circ$  ( $d = 0.42\text{ nm}$ ) from the (002) plane, magnified as an inset in figure 5a. Following reduction to rGO, this peak becomes weaker and much broader. This indicates that the graphene interlayer separation decreases for rGO films, consistent with the removal of the oxygen groups.

TGA curves of both films are given in figure 5b, which show two key stages of thermal modification at  $\sim 180$ – $230^\circ\text{C}$  and  $\sim 600$ – $700^\circ\text{C}$ . For the GO films, the first stage possibly reflects the decomposition or desorption of unstable or weakly bound oxygen groups, such as hydroxyl and carboxyl, or possibly of adsorbed water molecules. In contrast, rGO does not have these surface groups, and so the corresponding feature is absent from the TGA plot. The second stage at higher temperature is due to complete dehydroxylation and decomposition of the carbon structure that can be seen in SEM images following TGA studies

(supplementary figure S2). The weight-loss scenario beyond  $700^\circ\text{C}$ , seen with GO but much less so with rGO, can possibly be associated with the thermal destruction of a small number of tenacious residual oxygen-containing groups. The resulting total weight loss was 83.7 and 41.3% for GO and rGO, respectively.

Examples of WCA measurements on the two films can be seen in figure 6. For the GO film the droplet is hemispherical with a WCA of  $\sim 88^\circ$ , showing that the film is reasonably hydrophilic, as expected for a film with many oxygen-containing surface groups. Conversely, on the rGO film the water droplet is nearly spherical with a WCA of  $127^\circ$ , showing that this film is much more hydrophobic, consistent with a reduction of oxygen-containing surface groups.

#### 4. Conclusions

We have demonstrated the facile and rapid fabrication of hydrophobic rGO thin film via ESD. Film thickness and surface morphology are readily controlled by varying the composition of the sprayed suspension and the deposition time. Because this technique can easily be scaled to large areas, it provides a potential route to scaling up the fabrication of these thin films for commercial applications. The removal of oxygen functional groups and subsequent thermal treatment significantly increased the hydrophobic nature and thermal stability of the rGO surface. Having such a high density of structural defects, the rGO thin films may be promising candidates for the next generation of hydrophobic electrodes for use in supercapacitors and energy-storage applications. Follow-on experiments, such as hydrogenation or fluorination of the rGO surface, are planned to improve the hydrophobicity further.

#### Acknowledgements

RZ would like to thank the funding scheme of the Government of Republic of Kazakhstan under the Bolashak programme. OU and OT wish to acknowledge the support from the Ministry of Education and Science of the Republic of Kazakhstan under Grant No. AP08052848 and AP05135057.

#### References

- [1] Geim A K and Novoselov K S 2007 *Nat. Mater.* **6** 183
- [2] Balandin A A, Ghosh S, Bao W, Calizo I, Teweldebrhan D, Miao F *et al* 2008 *Nano Lett.* **8** 902
- [3] Felten A, Flavel B S, Britnell L, Eckmann A, Louette P, Pireaux J-J *et al* 2013 *Small* **9** 631
- [4] Park S and Ruoff R S 2009 *Nat. Nanotechnol.* **4** 217
- [5] Nine M J, Cole M A, Johnson L, Tran D N H and Losic D 2015 *ACS Appl. Mater. Interfaces* **7** 28482

- [6] Prasai D, Tuberkia J C, Harl R R, Jennings G K and Bolotin K I 2012 *ACS Nano* **6** 1102
- [7] Yoon H, Na S-H, Choi J-Y, Latthe S S, Swihart M T, Al-Deyab S S *et al* 2014 *Langmuir* **30** 11761
- [8] Huang Y, Li H, Wang L, Qiao Y, Tang C, Jung C *et al* 2015 *Adv. Mater. Interfaces* **2** 1400433
- [9] Wang J-N, Zhang Y-L, Liu Y, Zheng W, Lee L P and Sun H B 2015 *Nanoscale* **7** 7101
- [10] Stan M S, Nica I C, Popa M, Chifiriuc M C, Iordache O, Dumitrescu I *et al* 2019 *J. Ind. Text.* **49** 277
- [11] Geyer F, Schönecker C, Butt H-J and Vollmer D 2017 *Adv. Mater.* **29** 1603524
- [12] Peng C, Chen Z and Tawari M K 2018 *Nat. Mater.* **17** 355
- [13] Reina A, Jia X, Ho J, Nezich D, Son H, Bulovic V *et al* 2009 *Nano Lett.* **9** 30
- [14] Childres I, Jauregui L A, Tian J and Chen Y P 2011 *New J. Phys.* **13** 025008
- [15] Stankovich S, Piner R D, Nguyen S T and Ruoff R S 2006 *Carbon* **44** 3342
- [16] Sun H B, Yang J, Zhou Y Z, Zhao N and Li D 2013 *Mater. Technol.* **29** 14
- [17] Kymakis E, Stratakis E, Stylianakis M M, Koudoumas E and Fotakis C 2011 *Thin Solid Films* **520** 1238
- [18] Jaworek A 2007 *J. Mater. Sci.* **42** 266
- [19] Jaworek A and Sobczyk A T 2008 *J. Electrostat.* **66** 197
- [20] Varea A, Monereo O, Xuriguera E, Daniel Prades J and Cirera A 2017 *J. Phys. D: Appl. Phys.* **50** 315301
- [21] Schneider A, Uhlenwinkel V, Harig H and Bauckhage K 2004 *Mater. Sci. Eng. A* **383** 114
- [22] Konios D, Stylianakis M M, Stratakis E and Kymakis E 2014 *J. Colloid Interf. Sci.* **430** 108
- [23] Hummers W S and Offeman R E 1958 *J. Am. Chem. Soc.* **80** 1339
- [24] Park S, An J, Potts J R, Velamakanni A, Murali S and Ruoff R S 2011 *Carbon* **49** 3019
- [25] Gascho J L S, Costa S F, Recco A A C and Pezzin S H 2019 *J. Nanomater.* **2019** 1
- [26] Hu Y, Song S and Lopez-Valdivieso A 2015 *J. Colloid Interf. Sci.* **450** 68
- [27] Zhang H, Wang X, Li N, Xia J, Meng Q, Ding J *et al* 2018 *RSC Adv.* **8** 34241